Influence of Elastic Deformation on Single-Wall Carbon Nanotube Atomic Force Microscopy Probe Resolution

Ian R. Shapiro,[†] Santiago D. Solares,[‡,§] Maria J. Esplandiu,[†,⊥] Lawrence A. Wade,[||] William A. Goddard,*,[†,§] and C. Patrick Collier*,[†]

Jet Propulsion Laboratory and Departments of Chemistry, Chemical Engineering, and Applied Physics, California Institute of Technology, Pasadena, California 91125

Received: May 14, 2004

We have previously reported that 4−6 nm diameter single-wall carbon nanotube (SWNT) probes used for tapping-mode atomic force microscopy (AFM) can exhibit lateral resolution that is significantly better than the probe diameter when prone nanotubes are imaged on a flat SiO_2 surface. To further investigate this phenomenon, accurate models for use in atomistic molecular dynamics simulations were constructed on the basis of transmission electron microscopy (TEM) and AFM data. Probe−sample interaction potentials were generated by utilization of force fields derived from ab initio quantum mechanics calculations and material bulk and surface properties, and the resulting force curves were integrated numerically with the AFM cantilever equation of motion. The simulations demonstrate that, under the AFM imaging conditions employed, elastic deformations of both the probe and sample nanotubes result in a decrease of the apparent width of the sample. This behavior provides an explanation for the unexpected resolution improvement and illustrates some of the subtleties involved when imaging is performed with SWNT probes in place of conventional silicon probes. However, the generality of this phenomenon for other AFM imaging applications employing SWNT probes remains to be explored.

Introduction

To date, numerous papers have described the preparation of both multiwall and single-wall carbon nanotube (SWNT) atomic force microscopy (AFM) probes.[1−5] SWNT probes offer topographic imaging resolution superior to that of conventional silicon AFM tips, due to their unique chemical and mechanical properties, high aspect ratios, and molecular-scale dimensions.[6−10] In a recent publication we have described an efficient SWNT probe fabrication methodology and correlated the structures [acquired by transmission electron microscopy (TEM)] of 14 probes with the quality of AFM images they produced when imaging a prone SWNT sample.[11] By comparing the observed AFM resolution with the diameter of the probe nanotube measured from the TEM image, we found that the lateral resolution is on average 1.2 times the nanotube probe diameter. This value approaches the expected ideal ratio of unity in the absence of thermal vibrations and bending effects of the probe.[12]

Surprisingly, we have found that for some cases the apparent lateral resolution of the probe nanotube was actually *better* than expected on the basis of its diameter. In one case (shown in Figure 6 of ref 11), which forms the basis for the computational work presented here, we found that the lateral resolution from a 5.5 nm diameter SWNT probe was 1.2 nm, just 22% of the probe diameter. Here and in previous investigations, we define the lateral resolution of a SWNT probe as the difference between the measured height of a sample, which can be determined to
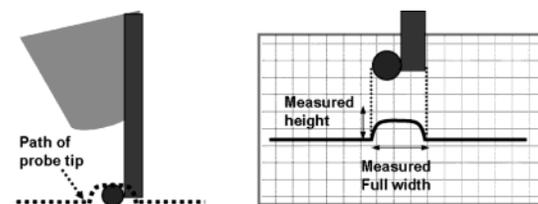

Figure 1. Schematic illustration of the relationship between probe diameter and lateral resolution. The left panel shows a model for a SWNT probe imaging a prone nanotube on a flat surface. The right panel shows the resulting cross-sectional profile, from which the width and height of the imaged nanotube are measured. In this simple geometric model, the full width is equal to the sum of the diameters of the probe and sample nanotubes.

high precision with AFM, and the measured diameter (full width at the noise floor), as outlined in Figure 1. In an ideal case, the limiting resolution equals the diameter of the probe. This simplified model, in which the probe and sample are considered to be incompressible objects, has commonly been used to describe AFM resolution.[2,4,5] However, simple geometrical arguments alone cannot explain the subdiameter resolution we observed. The potential for SWNT AFM probes to be used as common research tools requires a more thorough understanding of how the physical, chemical, and mechanical properties of SWNT probes affect image resolution.

To this end, we present here a quantitative atomistic molecular dynamics investigation of SWNT AFM probe behavior in the context of tapping-mode topographic imaging. The dimensions of the probes and samples are on the order of 1−50 nm, placing them within the range of atomistic simulations. To elucidate the actual tip−sample interactions that give rise to the observed phenomena, we have used TEM−AFM correlation data[11] to construct realistic molecular models of an open-ended SWNT probe interacting with a prone SWNT sample on a flat hydroxyl-

* Corresponding authors: e-mail collier@caltech.edu (C.P.C.), wag@wag.caltech.edu (W.A.G.).
† Department of Chemistry.
‡ Department of Chemical Engineering.
§ Materials and Process Simulation Center.
|| Department of Applied Physics and Jet Propulsion Laboratory.
⊥ Current address: Departament de Quimica, Universitat Autonoma de Barcelona, Barcelona, Spain.

TABLE 1: Tapping-Mode AFM Parameters Used for Numerical Simulations

cantilever spring constant	$k = 4.8$ N/m
cantilever quality factor	$Q = 150$
cantilever resonant frequency	$\omega/2\pi = 47.48$ kHz
free air oscillation amplitude	$A_0 = 39$ nm
amplitude set-point	$A_{sp} = 15.4$ nm
excitation force	$F_0 = 1.25$ nN

terminated silicon surface. These models were used to generate accurate potential curves at different positions of the probe relative to the sample. Integration of the resulting forces into the equation of motion for an oscillating cantilever yielded simulated topographic cross-section profiles that corroborate the experimental results. These simulations indicate that, under the AFM conditions employed, both probe bending and localized deformations of the probe and sample SWNTs strongly influence the topographic profile measured with AFM. The reversible elastic nature of these deformations is demonstrated both experimentally and in simulations.

Methods

Fabrication, characterization, and imaging with SWNT AFM probes has been described previously.[11] The effective lateral resolution of each probe was obtained by imaging, under ambient conditions in air, a carbon nanotube lying prone on a flat native-oxide silicon surface. To acquire accurate sample height and width measurements by use of amplitude-modulated AFM, it was necessary to first carefully calibrate the response of the system over a wide range of operational parameters, most importantly, the oscillation amplitude of the SWNT probe. For example, to understand the effects that vertical compression of a sample nanotube by the AFM probe had on the lateral resolution, repeated measurements of the sample nanotube height as a function of probe oscillation amplitude were performed for both conventional silicon and SWNT AFM tips. In all cases, the driving amplitudes employed were kept below the limit corresponding to a 10% reduction in the apparent height of the sample nanotube due to compression. In addition, we measured force calibration curves, which consist of scans of the damped oscillation amplitude as a function of the average tip–sample separation for a given cantilever driving force. The force calibration curves revealed the presence of coexisting attractive and repulsive tip–sample interaction regimes.[13,14] Bistable switching of the cantilever oscillation between the two regimes manifests itself as sudden changes in the observed sample height and width.[15] In general, we avoided these amplitude instabilities and the concomitant experimental artifacts by operating the AFM cantilever with a driving force sufficient to give a free-air oscillation amplitude greater than 20 nm. Consequently, all AFM data presented here can be considered in the repulsive regime or "intermittent contact" mode.

The simulation of the AFM tip motion was carried out by integration of the equation of motion for a damped harmonic oscillator at each AFM scan point on the sample, with the experimental parameter values contained in Table 1:

$$m\frac{d^2z(Z_c, t)}{dt^2} =$$

$$-kz(Z_c, t) + m\frac{\omega_0}{Q}\frac{dz(Z_c, t)}{dt} + F_{ts}(z_{ts}) + F_0\cos(\omega t) \quad (1)$$

where $z(Z_c, t)$ is the instantaneous tip position with respect to its average position (Z_c), k is the harmonic force constant for

the displacement of the tip with respect to its equilibrium rest position, m is the effective mass, $\omega_0 = \sqrt{k/m}$, the free resonant frequency, Q is the quality factor, z_{ts} is the instantaneous tip position *with respect to the sample*, $F_{ts}(z_{ts})$ the calculated tip–sample interaction force, and $F_0\cos(\omega t)$ is the oscillating driving force applied to the cantilever.

The use of this equation to describe the tip motion approximates the SWNT tip–cantilever ensemble as a point-mass harmonic oscillator. Nevertheless, this model has been used extensively for numerical treatment of tapping-mode AFM with conventional probes. Although the actual dynamics of the oscillating cantilever in the presence of the probe–sample interactions are nonlinear, the validity of the harmonic approximation for modeling conventional tapping-mode AFM imaging in air has been demonstrated with both theory and experiment for the range of parameters used here.[13,16–19]

Prior to integrating eq 1 we obtained the required tip–sample interaction forces using atomistic models, as explained in detail below. All molecular dynamics (MD) simulations were carried out with Cerius2 molecular simulations software (Accelrys, San Diego, CA). The MD force-field parameters were optimized by fitting the material bulk and surface properties such as elasticity moduli, vibrational frequencies, and surface geometry both to experimental data and to rigorous quantum mechanics calculations on clusters representative of the silicon and graphene systems under study. Equation 1 was integrated by use of the Verlet algorithm to fourth-order accuracy for the tip position and second-order accuracy for the tip velocity.[20]

Realistic atomistic models were constructed for the SWNT probe used for tapping-mode AFM imaging. Every effort was made to match the model structures and simulation conditions as closely as possible to corresponding experimental values, including the nanotube probe diameter, length, angle relative to the substrate normal, and the fine structure at the probe end. All silicon surfaces were (100) and were terminated with hydroxyl groups. The probe was a (40,40)[21] armchair SWNT (5.4 nm diameter, 45 nm length, with 5 nm of fixed atoms at one end of the probe to simulate its attachment site at the AFM tip) constructed from approximately 25 000 carbon atoms. The sample was a (16,16) armchair SWNT (2.2 nm diameter, 10 nm length) constructed from approximately 2600 carbon atoms. The sample SWNT was kept fixed at both ends during the calculations to simulate a very long nanotube, which is unlikely to displace laterally during AFM tapping. Similar models were generated for a conventional silicon tip interacting with the sample nanotube. Several of these models are shown in Figure 2.

The tip–sample interaction potentials were constructed by vertically approaching the sample with the probe nanotube at 0.05 nm intervals, at each point optimizing the system geometry by minimization of the potential energy (additional calculations performed at 300 K showed that the potentials did not significantly change with inclusion of thermal vibrations at room temperature; see Supporting Information). The gradient of this energy–position function with respect to the vertical tip position is the tip–sample interaction force.

To reduce the computational cost of the molecular simulations, each model of a nanotube on the surface included only a small section of the silicon surface, sufficient to obtain an accurate description of the SWNT probe interactions with the sample. This does not give an accurate description of the interaction of the tip with the silicon surface for the cases in which the SWNT tip deforms and slips against one side of the sample nanotube and makes contact with the underlying
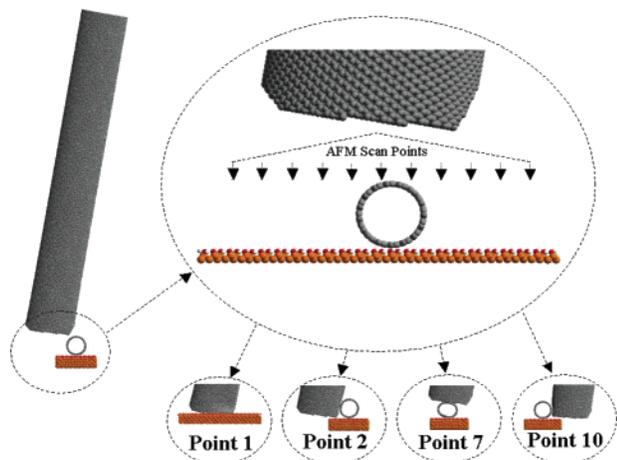
Elastic Deformation and SWNT AFM Probe Resolution

J. Phys. Chem. B, Vol. 108, No. 36, 2004 **13615**

Figure 2. Illustration of the models used to construct the tip−sample interaction profile. The models were constructed on the basis of experimental TEM and AFM data. The final tip position during the AFM scan is shown for four of these points. The corresponding force curves are shown in Figure 3.

substrate. To correct this, another model was constructed *without* a sample nanotube on the substrate to obtain the interaction forces between the tip and the bare silicon surface. The deformation of the tip was considered in all cases when the relative position of the surface and the end of the tip was calculated for each scan point.

This procedure provides a discrete set of points, and so regression analysis with simple functional forms (e.g., polynomials or functions of the form $1/r^n$) was performed in order to obtain continuous force−position curves, which can be programmed easily into the AFM dynamics integration code. The forces for a given vertical position of the tip may have different values, depending on whether the tip has slipped relative to the sample SWNT. This was accounted for during the construction of the force−position curves and incorporated into the integration of the cantilever equation of motion.

Results and Discussion

A series of 11 curves showing probe−sample force versus height were generated at evenly spaced points along the line perpendicular to the axis of the sample nanotube. The separation between adjacent points was 1 nm. Figure 2 shows the location of the 11 scan points relative to the sample nanotube, and four of the corresponding tip−sample force curves are shown in Figure 3 (all 11 energy-position curves, from which these force curves were obtained by differentiation, are provided in the Supporting Information). The abscissa on all graphs in Figure 3 corresponds to the distance between the lowest atom on the SWNT tip and the highest atom of the Si(100)−OH surface. Negative values on this axis correspond to elastic deformations in nanotube and surface geometry, including local deformation of the probe, as well as slight deformation of the Si−OH surface.

Each of the 11 probe−sample force curves generated along the scan line was then inserted into eq 1 and integrated for the average tip positions relative to the substrate (Z_c) ranging from 50 to 0 nm, by use of actual imaging parameter values.[11] For each scan point and tip position, eq 1 was integrated numerically for 0.02 s with a 0.1 ns integration step (to fourth-order accuracy with respect to the time step size) to determine the oscillation amplitude of the cantilever as a function of its vertical position [the initial tip position was set equal to its equilibrium position, i.e., $z(Z_c, 0) = 0$, and the initial velocity was set to zero in all cases]. This numerical procedure is analogous to acquiring a "force calibration curve" for each scan point in Figure 2.

The result of these calculations was a curve showing the cantilever equilibrium oscillation amplitude as a function of the average vertical position of the tip for each point along the scan direction. Two of these curves are shown as insets in Figure 5. The simulated cross-section trace in Figure 5 was then constructed by plotting the locus of tip position values which maintained the oscillation amplitude at the set-point value of 15.4 nm. Note that the average tip−sample separation for each scan point is given relative to the value obtained when imaging the bare silicon oxide substrate.

The construction of tip−sample interaction force curves through molecular simulations of large finite systems underestimates the long-range attractive forces present in the system. This is because the calculation of nonbonded interaction energies between pairs of atoms is generally limited to a cutoff radius on the order of 1 nm or less to reduce the cost of the computation (the number of nonbonded interactions, which scales with the square of the number of atoms in the simulation, can account for over 90% of the computation costs of a typical system). Underestimating the long-range attractive forces, and hence the region of positive force gradient, can alter the predicted regions of amplitude bistability.[13] However, at the free oscillation amplitude employed here, $A_0 = 39$ nm, the average force will be determined almost exclusively by the repulsive part of the tip−sample interaction potential,[16] and thus the underestimation of the attractive contribution will have negligible influence on the simulated topographic profile.

Under ambient conditions, a thin film of water is adsorbed on hydrophilic surfaces such as SiO_2. The formation of a meniscus or liquid bridge between the surface and the probe will result in an additional attractive capillary force that depends on probe−sample distance.[22] We did not include the effects of adsorbed water in our model. We do not expect that inclusion of these effects will significantly change the nanoscopic interactions between the probe and sample nanotubes predicted by the simulations. Future work will address this issue.

Simple models of AFM resolution assume that the probe is a rigid, incompressible cylinder with a flat or hemispherical end. In practice this is not the case. High-magnification TEM images show that the ends of the probe nanotubes are generally open due to ablation from an electrical etching procedure used to shorten the nanotube probes to useful lengths.[2,4] Purely geometric arguments suggest that an open-ended tube with protruding asperities could, for extremely low-relief samples, provide resolution comparable to the asperity diameter rather than the full diameter of the probe, in direct analogy to results published for silicon probes.[23] However, probe asperities are unlikely to be important when imaging a sample nanotube that has a diameter (height above the surface) comparable to that of the probe.

The Young's modulus of SWNTs is approximately 1.25 TPa along the tube axis.[24] Because of this very high stiffness, only a small amount of longitudinal compression of the tube occurs during AFM imaging. However, Snow et al.[12] have shown that SWNT probes are susceptible to bending due to their high aspect ratio if not oriented vertically relative to a surface. Image artifacts from bending can be minimized by shortening the nanotube probe so that it protrudes less than 100 nm beyond the supporting silicon tip.

While SWNTs have exceptional longitudinal stiffness, radially they are far more compliant,[25] a characteristic that permits localized deformation of the nanotube walls. The likelihood of deformation is further increased due to the structural discontinu-
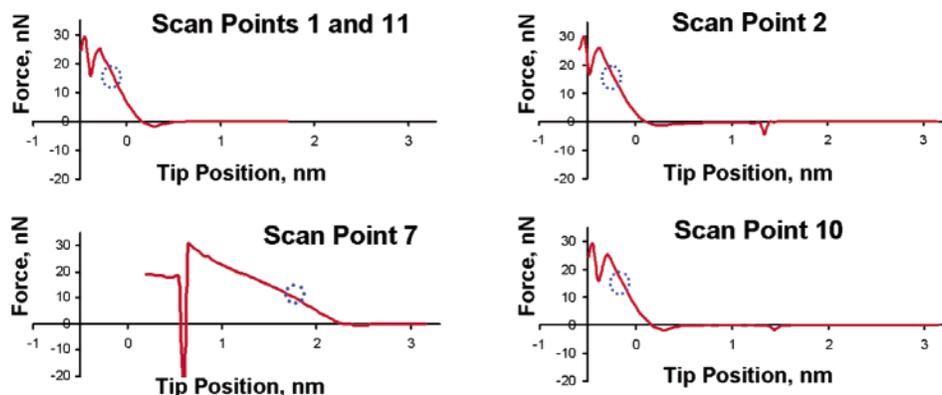
Figure 3. Tip−sample force curves calculated for four of the 11 scan points shown in Figure 2. The abscissa on all graphs corresponds to the distance between the lowest atom on the SWNT tip and the highest atom of the Si(100)−OH surface. The small blue circle in each plot indicates the lowest position that the probe tip reached during the subsequent AFM imaging simulation.
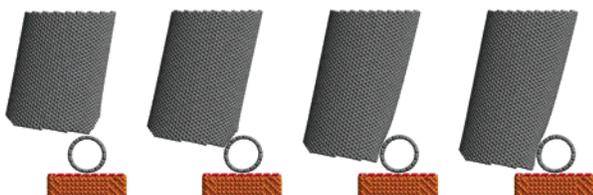

Figure 4. Illustration of the slipping phenomenon of the SWNT probe past the SWNT sample for scan point 3. Both bending along the length of the probe and local deformation contribute to slipping. The picture shows that the simulated probe is more susceptible to deformation, although the sample nanotube does deform slightly. This is due to the larger diameter of the probe (5.4 vs 2.2 nm) and the fact that its end is opened, which decreases its radial rigidity.

ity at the opened end of the nanotube probe. The susceptibility of nanotubes to radial deformation is predicated upon two competing effects: the energy cost associated with strain of the nanotube as it is deformed from its equilibrium cylindrical geometry, and the stabilization that a compressed nanotube gains due to increased interlayer van der Waals attractions. These two competing effects scale in opposite directions with increased nanotube diameter, such that larger SWNTs are easier to deform radially than smaller diameter tubes.[26] We have previously observed that SWNTs attached to silicon AFM tips via the "pick-up" method tend to be 4−6 nm, which is larger than the tubes observed lying prone upon the pick-up substrate (1−3 nm).[11] We postulated that the increase in net binding energy with larger diameter nanotubes stems from the interplay between van der Waals forces and the geometric stiffness of a nanotube. The resulting radial "softness" of these larger nanotubes not only increases the energy with which they bind to a silicon probe during pick-up but also has significant implications when they are subsequently used for AFM imaging.

Our molecular dynamics simulations show lateral slipping of the probe nanotube relative to the sample nanotube, due both to bending along the length of the probe and to localized radial deformation of the probe and sample at the point of contact (illustrated in Figure 4 and Supporting Information). This behavior is a function of the structures and relative orientations of the probe and sample nanotubes, the applied tip−sample force, and the position (in the x−y plane) of the probe nanotube relative to the sample nanotube. The smaller the x−y distance between the center of the probe tube and the axis of the sample tube, the larger the force required to deform the nanotubes and cause them to slip past one another. That is, when the probe presses on the edge of the sample nanotube, a smaller amount of force is required to cause it to slip laterally than when it

presses on the crown of the sample nanotube. The simulations show this deformation behavior to be completely reversible and elastic (images illustrating reversibility are provided in the Supporting Information). Experimentally, the elasticity is demonstrated by the fact that we have not observed the topographic cross sections to change significantly during imaging at a given amplitude set-point, and the TEM images taken of each probe after AFM imaging show no alterations of the nanotube structure, such as kinks or buckles.

This lateral slipping and deformation of the probe nanotube explains the observation of sub-probe-diameter effective resolution. In amplitude−feedback tapping-mode AFM, modulation of the cantilever oscillation amplitude depends on the average strength of the tip−sample forces.[27] The AFM controller adjusts the extension of the z-piezoelectric element in order to hold the amplitude of the cantilever oscillation at the fixed value designated by the amplitude set-point (an independent variable set by the user). The resulting z-piezo voltage corrections are converted to units of length and output as the topographic height data. If the probe and sample deform negligibly under the associated tapping forces, the sample height can be measured accurately to within the precision of the piezoelectric element, typically <1 Å. However, if either material is significantly deformable, the resultant z-piezo data represents a more complex convolution of probe and sample structure.

The simulations conducted here indicate that when the probe SWNT is tapping on an edge of the sample SWNT, the subsequent repulsive forces deform *both* nanotubes sufficiently to allow them to slip past one another without significantly influencing the cantilever oscillation amplitude. In fact, when the very edges of the probe and sample tubes come into contact, the net tip−sample force is actually attractive rather than repulsive, due to the large area of favorable contact between the graphitic surfaces. This is illustrated in the force curves for scan points 2 and 10 by the fact that the net force is negative between the two local minima, corresponding to the region in which the probe and the sample are slipping past one another. Once lateral slipping takes place, the resulting tip−sample interaction is dominated by the repulsive forces between the probe SWNT and the Si/SiO$_2$ surface. Thus, for that particular x−y position, the AFM controller does not "see" the sample nanotube. Only when the probe SWNT is positioned closer to the crown of the prone sample SWNT are the interaction forces between the probe and sample nanotubes high enough to cause sufficient damping of the cantilever oscillation amplitude. At scan point 7, which corresponds to the probe tapping on the crown of the sample nanotube, no slipping can take place under
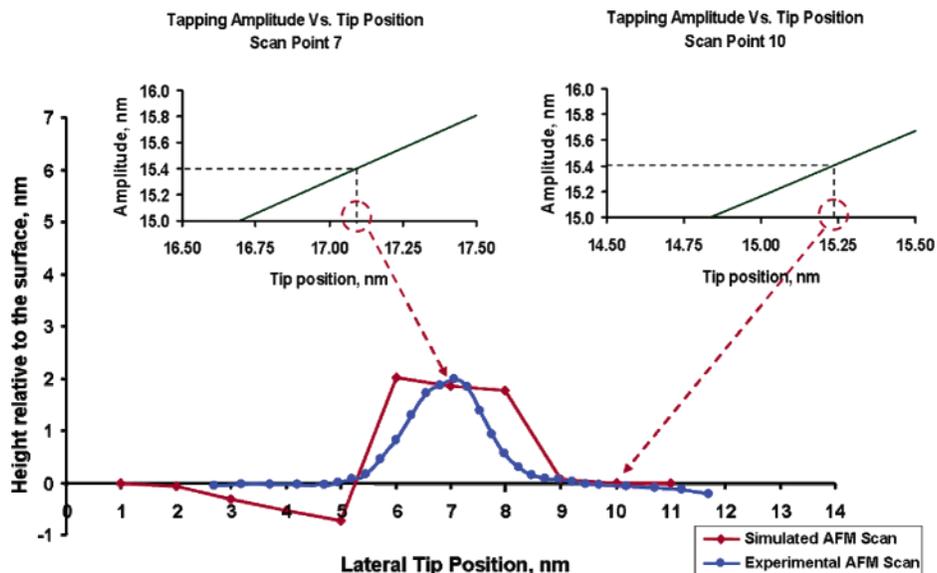
Elastic Deformation and SWNT AFM Probe Resolution

J. Phys. Chem. B, Vol. 108, No. 36, 2004 **13617**

Figure 5. Schematic depiction of the construction of an AFM scan from molecular and AFM dynamics simulations. The two inset amplitude−distance curves illustrate how the measured height is obtained for each scan point at an amplitude set-point of 15.4 nm. The resulting AFM cross-sectional height is given relative to the average tip separation from the bare SiO$_2$ surface. The horizontal axis corresponds to the scan points shown in Figure 2. For comparison, the cross section from experimental data has been overlaid on the same scale with its center point arbitrarily positioned to match up with the center of the simulated cross section.

the imaging conditions given in Table 1, because the maximum tip−sample repulsive force does not exceed the necessary threshold, ∼30 nN. Here, the cantilever amplitude is damped by the sample nanotube and the AFM records the interaction. The net result is that the topographic data indicates an apparent nanotube width that is smaller than the sum of the probe and sample SWNT diameters.

A quantitative representation of this phenomenon is illustrated in Figure 5. The lower half of the figure shows the effective cross section of a sample nanotube, calculated from the MD and AFM dynamics simulations, obtained when a SWNT probe is used under the repulsive tapping conditions given in Table 1. This scan shows two important features that are also observed experimentally. First, the apparent probe resolution for this simulation is 2.0 nm, 37% of the probe diameter. Additionally, the simulated cross section is asymmetric, which is a direct consequence of the specific SWNT probe geometry, particularly the tilt angle, that favors probe−sample slipping more on one side of the sample than on the other.

In contrast, MD simulations have shown that a conventional silicon probe does not slip under the same imaging conditions. This is because the rigidity of the silicon probe requires higher forces to induce deformation, while the larger radius of curvature of the probe tip actually generates smaller lateral forces compared to a SWNT probe. The different behavior is also due to the chemical properties of crystalline silicon, which strongly influence the surface−surface interactions with the SWNT sample, as well as the attractive van der Waals forces between the larger silicon tip and the silicon surface. These two parameters in particular, probe compressibility and adhesion forces, are transformed in a highly nonlinear way by the response of the oscillating tip.[28] Thus, SWNT probes perform in a fundamentally different manner than silicon probes, not merely when imaging prone carbon nanotubes but for a variety of samples.

We have also simulated a smaller diameter SWNT probe since previous reports have described nanotube probes in the 1−3 nm diameter range.[1,2,4,7] Smaller diameter nanotube probes should be far less susceptible to localized radial deformation,

due to their increased resistance against compression (as seen with the sample nanotube, Figure 4). However, the bending mode along the length of a thinner probe is actually softer, since the flexural rigidity scales as r^4.[29] The probe was a (16,16) armchair SWNT (2.2 nm diameter, 20 nm length) that had approximately the same aspect ratio as the larger 5.4 nm probe used in this study. As before, the probe nanotube was oriented at 15° relative to the surface normal and the sample nanotube was 2.2 nm in diameter and 10 nm in length. Images from the simulation are incorporated in the Supporting Information and show that slipping also occurs for the thinner probe when tapping on the edge of the sample nanotube. For this probe, the slipping is almost entirely due to bending and not to local deformation. The corresponding tip−sample force curve indicates that the force opposing the slipping motion of the probe was negligible.

Dekker and co-workers[30] have reported previously that as a function of driving amplitude in tapping-mode imaging, a conventional silicon AFM probe can vertically compress a 1.4 nm single-wall nanotube lying on a flat surface, resulting in a decreased apparent *height*. This experimental observation is consistent with previously reported experimental measurements and molecular dynamics simulations, which described radial deformation of 1−3 nm single-wall carbon nanotubes by both van der Waals forces and external static loads.[31−33] Here we show that in tapping-mode AFM, the associated forces deform the probe nanotube in addition to the sample, strongly influencing the subsequently measured effective *lateral* resolution.

Our molecular dynamics simulations confirm that some vertical compression of a prone sample nanotube occurs under standard tapping-mode AFM conditions, for both conventional silicon AFM probes and SWNT probes. However the simulations predict that this effect is, at most, 10% of the sample tube diameter for 1−3 nm SWNTs and occurs primarily when the probe nanotube is tapping on the crown of the sample nanotube (see, for example, point 7 in Figure 2). This corresponds well with our experimental calibration of sample tube compression under the tapping-mode operating parameters employed. The enhanced lateral resolution, on the other hand, is due to the

highly localized deformation and bending of the probe nanotube along the edges of the sample nanotube, and is therefore not affected significantly by vertical compression.

Conclusion

By correlating experimental data with atomistic molecular dynamics simulations, we have characterized how the unique properties of SWNT AFM probes can strongly influence topographic imaging fidelity. Probe bending and mutual local deformation of both the probe and sample nanotubes under typical tapping-mode AFM forces can result in a reduction of the measured width of the sample tube, and consequently an ostensive improvement of the lateral resolution, to the extent that the resolution can appear to be better than expected from the measured diameter of the nanotube probe. We are interested in determining whether a similar improvement of apparent resolution is observed when imaging less compliant samples of different material composition, such as metallic or semiconducting nanoparticles.

Given the interest in nanoscale physical and biological phenomena, SWNT probes are likely to evolve into a more common research tool. A complete understanding of probe behavior in the context of atomic force microscopy is therefore critical. It is important to note that the lateral resolution reported here is an apparent value, arising from the simplified definition set forth in the Introduction, and was studied for the specific case of 4−6 nm diameter open-ended SWNT probes imaging 2−3 nm diameter SWNTs adsorbed on a flat surface. In practice, the resolving power of an AFM probe is dependent upon the experimental context. It is of particular importance to determine whether the observed deformation phenomenon results in a net gain or loss of structural information when SWNT probes are used to image soft nanoscale samples, such as biological macromolecules. The improvement in the apparent resolution due to deformation of the probe and sample nanotubes in this study was a consequence of the relatively high driving forces applied to the AFM cantilever. Tapping-mode AFM imaging performed in this repulsive regime with conventional probes has been shown to damage biomolecules.[14] In addition, resolution less than the probe diameter could complicate interpretation of AFM images quantitatively.

The combination of probe structure determination, characterization of imaging resolution, and simulated dynamic behavior described here has highlighted practical differences between carbon nanotube probes and conventional silicon probes. This work also underscores the usefulness of atomistic simulations in describing the dynamic nanoscale interactions involved in scanning probe microscopy.

Supporting Information Available: Simulated energy−distance and force−distance curves, force-field parameters, effects of thermal vibrations, illustrations of bending and local deformation modes of a 5.4 nm diameter SWNT probe, of lateral slipping of a 2.2 nm diameter SWNT probe, and the elastic nature of nanotube deformation. This material is available free of charge via the Internet at http://pubs.acs.org.

References and Notes

(1) Cheung, C.-L.; Hafner, J. H.; Odom, T. W.; Kyoungha, K.; Lieber, C. M. *Appl. Phys. Lett.* **2000**, *76*, 3136.

(2) Wong, S. S.; Wooley, A. T.; Joselevich, E.; Cheung, C. L.; Lieber, C. M. *J. Am. Chem. Soc.* **1998**, *120*, 8557.

(3) Campbell, P. M.; Snow, E. S.; Novak, J. P. *Appl. Phys. Lett.* **2002**, *81*, 4586.

(4) Hafner, J. H.; Cheung, C. L.; Oosterkamp, T. H.; Lieber, C. M. *J. Phys. Chem. B* **2001**, *105*, 743.

(5) Choi, N.; Uchihashi, T.; Nishijima, H.; Ishida, T.; Mizutani, W.; Akita, S.; Nakayama, Y.; Ishikawa, M.; Tokumoto, H. *Jpn. J. Appl. Phys.* **2000**, *39*, 3707.

(6) Dai, H.; Hafner, J. H.; Rinzler, A. G.; Colbert, D. T.; Smalley, R. E. *Nature* **1996**, *384,* 147.

(7) Wong, S. S.; Woolley, A. T.; Odom, T. W.; Huang, J.-L.; Kim, P.; Vezenov, D. V.; Lieber, C. M. *Appl. Phys. Lett.* **1998**, *73*, 3465.

(8) Hafner, J. H.; Cheung, C. L.;. Wooley, A. T.; Lieber, C. M. *Prog. Biophys. Mol. Biol.* **2001**, *77*, 73.

(9) Stevens, R. M. D.; Frederick, N. A.; Smith, B. L.; Morse, D. E.; Stucky, G. D.; Hansma, P. K. *Nanotechnology* **2000**, *11*, 1.

(10) Nguyen, C. V.; Stevens, R. M. D.; Barber, J.; Han, J.; Meyyapan, M. *Appl. Phys. Lett.* **2002**, *81*, 901.

(11) Wade, L. A.; Shapiro, I. R.; Ma, Z.; Quake, S. R.; Collier, C. P. *Nano Lett.* **2004**, *4*, 725.

(12) Snow, E. S.; Campbell, P. M.; Novak, J. P. *Appl. Phys. Lett.* **2002**, *80*, 2002.

(13) García, R.; San Paulo, A. *Phys. Rev. B* **1999**, *60*, 4961.

(14) San Paulo, A.; García, R. *Biophys. J.* **2000**, *78*, 1599.

(15) García, R.; San Paulo, A. *Phys. Rev. B* **2000**, *61*, R13381.

(16) San Paulo, A.; García, R. *Phys. Rev. B* **2002**, *66* R041406.

(17) San Paulo, A.; García, R. *Phys. Rev. B* **2001**, *64*, 193411.

(18) Rodriguez, T. R.; García, R. *Appl. Phys. Lett.* **2002**, *80*, 1646.

(19) Cleveland, J. P.; Anczykowski, B.; Schmid, A. E.; Elings, V. B. *Appl. Phys. Lett.* **1998**, *72*, 2613.

(20) For an explanation of (*n*, *m*) designation, see Jeroen, W. G.; Wildoer, L. C.; Venema, A. G.; Rinzler, R.; Smally, E.; Dekker, C. *Nature* **1998**, *391*, 59.

(21) Frenkel, D.; Smit, B. *Understanding Molecular Simulation*; Academic Press: San Diego, CA, 2002; pp 69−71.

(22) García, R.; Calleja, M.; Rohrer, H. *J. Appl. Phys.* **1999**, *86*, 1898.

(23) Engel, A.; Müller, D. *Nat. Struct. Biol.* **2000**, *7*, 715.

(24) Krishnan, A.; Dujardin, E.; Ebbesen T. W.; Yianilos, P. N.; Treacy, M. M. J. *Phys. Rev. B* **1998**, *58*, 14013.

(25) Shen, W.; Jiang, B.; Han, B. S.; Xie, S.-S. *Phys. Rev. Lett.* **2000**, *84*, 3634.

(26) Gao, G.; Çağin, T.; Goddard, W. A. *Nanotechnology* **1998**, *9*, 184.

(27) García, R.; Perez, R. *Surf. Sci. Rep.* **2002**, *47*, 197.

(28) Lee, S. I.; Howell, S. W.; Raman, A.; Reifenberger, R. *Phys. Rev. B.* **2002**, *66*, 115409.

(29) Wilson, N. R.; Macpherson, J. V. *Nano Lett.* **2003**, *3*, 1365.

(30) Postma, H. W. C.; Sellmeijer, A.; Dekker, C. *Adv. Mater.* **2000**, *12*, 1299.

(31) Hertel, T.; Walkup, R. E.; Avouris, P. *Phys. Rev. B* **1998**, *58*, 13870.

(32) Li, C.; Chow, T.-W. *Phys. Rev. B* **2004**, *69*, 073401.

(33) Ruoff, R. S.; Tersoff, J.; Lorents, D. C.; Subramoney, S.; Chan, B. *Nature* **1993**, *364*, 514.